Dyes and Pigments 81 (2009) 103–112

Contents lists available at ScienceDirect

Dyes and Pigments

journal homepage: www.elsevier.com/locate/dyepig

The adsorption behavior of C.I. Acid Blue 9 onto calcined Mg–Al layered double hydroxides

Anthony R. Auxilio, Philip C. Andrews, Peter C. Junk, Leone Spiccia*

CRC Smartprint and School of Chemistry, Monash University, Victoria 3800, Australia

ARTICLE INFO

Article history:
Received 7 September 2008
Received in revised form 24 September 2008
Accepted 24 September 2008
Available online 7 October 2008

Keywords:
Layered double hydroxides
Inorganic pigments
Calcination
Mesoporous materials
Acid Blue 9
Adsorption
Textural properties

ABSTRACT

Mesoporous calcined Mg–Al layered double hydroxides with different Mg/Al molar ratios were investigated for their ability to adsorb the commercial dye, C.I. Acid Blue 9, with a view to exploring their suitability as inorganic pigments in Ink Receptive Layer formulation. Uptake capacity was characterized using the Langmuir model and the resulting L-2/H-2 type plots indicated that the acid dye anions were adsorbed onto the surface by strong interactions. Optimum dye adsorption was achieved for a Mg/Al molar ratio ≈5.6. A surface adsorption mechanism is proposed to account for the adsorption of the dye onto the calcined Mg–Al layered double hydroxides. X-ray powder diffraction analysis indicated that given sufficient time it is possible to intercalate the dye within the layered double hydroxides' interlayer via a reconstruction mechanism. Scanning electron microscopy, N_2 adsorption–desorption analysis and helium pycnometry were employed to examine the textural properties of the materials, which were correlated with their adsorption properties.

1. Introduction

For several decades there has been a major expansion in the development of new nanoporous materials. One class of materials that have attracted interest are the pillared clays and their calcined products [1]. Some of the major applications of these materials are as adsorbents for air [2] and water [3–9] pollutants, in fuel cell technology [10] and for paper coatings [11–14]. In particular, the calcined layered double hydroxides (LDHs) are being intensively studied due to their high anion capacity [9], reusability [15], larger surface area, porosity and basic properties [16]. Among the various types of LDH species, a hydrotalcite-like compound consisting of a Mg–Al layered double hydroxide with carbonate as an interlayer anion is commonly used for a variety of applications. The composition of this material can be represented as $[Mg_{1-x}Al_x(OH)_2]^{x+}[(CO_3{}^{2-})_{x/2}\cdot mH_2O]$, where $CO_3{}^{2-}$ is an exchangeable anion, and x is the trivalent metal ratio, $Al^{3+}/(Mg^{2+}+Al^{3+})$ determines layer charge density. Rives [17] has noted that the structure of LDHs collapse upon heating even at rather moderate temperatures, leading to crystalline, three-dimensional phases. The precise nature of this material depends on several factors, such as the atmosphere surrounding the sample during the decomposition, the presence of oxidisable or reducible cations in the brucite-like layers and the nature of the interlayer anion. In the case of Mg–Al- LDHs with carbonates as interlayer anions, heating the material at ca. 100 °C results in the removal of physisorbed water while further heating between 140 and 260 °C removes the interlayer water molecules. As the temperature is increased to 450–500 °C, decarbonation and dehydroxylation can take place resulting in the formation of MgO (periclase), whose lattice parameters are smaller than those for pure MgO due to the inclusion of Al^{3+} in the MgO lattice forming a solid solution. Finally, at a very high temperature, e.g., 1000 °C, the calcination products may include a mixture of MgO and Al_2O_3 (alumina) or MgO and $MgAl_2O_4$ (spinel). Ulibarri et al. [18] noted that calcination at temperatures above 700 °C induces phase separation and the original layered structure does not reconstruct.

The adsorption and intercalation of C.I. Acid Blue 9 on Mg–Al layered double hydroxides of variable Mg–Al molar ratio compositions were reported by the present authors [19]. These authors also explored the adsorption behavior of dyes commonly used in inkjet printing, such as C.I. Acid Blue 9, C.I. Acid Yellow 23 and C.I. Acid Red 37 on the functionalized pseudo-boehmite [20]. In the present work, the ability of calcined LDH materials of variable Mg/Al ratios to adsorb C.I. Acid Blue 9 (AB9) is explored with a view to assessing their suitability for use as inorganic pigments in Ink Receptive Layer (IRL) formulations for application in inkjet printing. AB9 has many important applications [19] and, in this study, it has been selected because it is widely used as the cyan component in

* Corresponding author. Tel.: +61 3 9905 4526; fax: +61 3 9905 4597.
E-mail address: leone.spiccia@sci.monash.edu.au (L. Spiccia).

0143-7208/$ – see front matter © 2008 Elsevier Ltd. All rights reserved.
doi:10.1016/j.dyepig.2008.09.011

inkjet inks, either alone or in combination with other cyan dyes [22].

To the best of our knowledge, there are no previous studies of the C.I. Acid Blue 9 adsorption properties on calcined Mg–Al-LDH-CO_3. Detailed characterization of these mesoporous materials obtained following calcination of the LDHs has been carried out using powder X-ray diffraction analysis, scanning electron microscopy, FT-IR and TGA analyses, BET measurements and He pycnometry and the results were used to rationalize the dye adsorption.

2. Materials and methods

2.1. Synthesis of calcined Mg–Al-LDH-CO_3 (CLDH)

Precursor Mg–Al-LDH-CO_3 (LDH) materials with varying Mg^{2+}/Al^{3+} ratios (2.0–10.0) were prepared at pH 9.50 (±0.05) by the co-precipitation method described previously [19]. These precursor materials were fired at 500 °C under air atmosphere for 6 h using a BTC-9090 furnace. At this temperature, the LDH starting material is fully calcined. This is necessary to avoid complication in the interpretation of the adsorption data that arises if the original LDH material is present. The calcined products were used directly in characterization and dye adsorption experiments.

2.2. Adsorption experiments

A 1.85 mM solution of C.I. Acid Blue 9 (C.I. 42090, Erioglaucine, disodium bis[4-(*N*-ethyl-*N*-3-sulfonatophenylmethyl)aminophenyl]phenylmethylium) obtained from Saujanya Dyechem (Fig. 1) was prepared using two different solvent systems: (1) 20% (v/v) glycerol–H_2O; and (2) pure water. The dye content in the commercial product (85%) was taken into account in the calculation of the dye concentration. The glycerol-containing solvent system was included in order to mimic the commercial inkjet ink that may contain humectants and dye solubilizer such as glycerol. The dye was used without further purification. The wavelength at maximum absorbance ($\lambda_{max} = 629$ nm) and molar absorptivity ($\varepsilon = 1.37 \times 10^5\ M^{-1}\ cm^{-1}$) values were determined experimentally. This dye concentration is a typical concentration used in many inkjet inks, such as BCI Canon [22].

CLDH materials were subjected to a dye affinity test (in triplicate) according to published methodology [19]. Briefly, AB9 solution (1.85 mM, 5.00 mL) was added to the pigment (0.500 g) in a centrifuge tube. The tube was agitated using a vortex mixer for 1 min followed by centrifugation (5000 rpm, 5 min). The supernatant liquid was removed carefully. An aliquot of supernatant liquid was diluted with distilled water so that the final absorbance reading was in the range of 0.5–1.0. For a selection of CLDH systems that exhibited excellent dye affinity (>99% of dye adsorbed from the standard solution), adsorption isotherms were constructed as discussed in previous publications [19,20]. Briefly, varied amounts of CLDH materials (1.0–0.05 g) were exposed to a constant dye concentration and, following adsorption, the supernatant liquids were analyzed in the same manner as for the dye affinity test. Triplicate analyses were conducted in all cases. The data were analyzed by the application of the Langmuir equation [5] originally derived for gas adsorption on planar surfaces [21], $C_s = C_m K_a C_p / (1 + K_a C_p)$, where C_s (mmol/g) is the amount of dye adsorbed onto the surface, C_p (mmol/mL) is the amount of dye remaining in the solution, C_m (mmol/g) is the maximum adsorption capacity at a monolayer coverage, and K_a (M^{-1}) is the equilibrium binding constant.

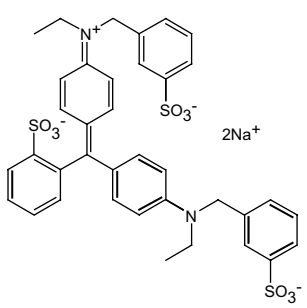

Fig. 1. Structure of disodium salt of Acid Blue 9.

2.3. Characterization

Powder X-ray diffraction analysis was performed using a Philips 1140 diffractometer under the following conditions: 40 kV, 25 mA, CuKα ($\lambda = 0.15406$ nm) radiation. The samples, as unoriented powders, were scanned in steps of 0.02° (2θ) in the range from 2 to 70° at a speed of 2°/min.

Metal analyses were performed using atomic absorption spectrometry (AAS) using a VARIAN SpectrAA – 400 spectrophotometer. Mg and Al concentrations were based on the Mg–Al-LDH-CO_3 precursor materials previously [19] obtained through AAS. The metal ratio was assumed to remain unchanged after firing.

Infrared experiments were carried out using an EQUINOX – IFS 55 spectrometer. Samples were mixed with KBr to produce a disc with a 1% compound loading. The spectra were recorded between 4000 and 400 cm^{-1} at a resolution of 2 cm^{-1}.

Thermogravimetric analyses were performed on a Perkin–Elmer Pyris 1 TGA instrument. Samples (5–10 mg) were heated in a platinum crucible between 30 and 800 °C at a heating rate of 10 °C/min under a stream of nitrogen.

Surface morphologies and particle size were studied using a Philips XL30 Field Emission Scanning Electron Microscope manufactured by Oxford Instruments at 5 kV.

Surface area, pore size, and pore volume were studied using an Omnisorp 360 CX analyzer manufactured by Coulter. The samples were degassed at 378 K prior to analyzing using nitrogen adsorption–desorption at 77 K.

The density was determined by helium pycnometry using an AccuPyc 1330 gas displacement pycnometer manufactured by Micromeritics. Prior to density measurements and to ensure the samples were extremely dry, all calcined products were immediately placed in a desiccator and left overnight.

3. Results and discussion

3.1. General characterization

With increasing Mg/Al molar ratio, the intensities of the MgO (*JCPDS #: 30-794*) reflections at 2θ values of 36.9°, 42.9° and 62.2° (*single asterisk*) increase (see Supplementary information). This implies a greater amount of microcrystalline MgO. As shown previously, the formation of hydromagnesite [$Mg_5(CO_3)_4(OH)_2 \cdot 5H_2O$] could not be avoided at the higher Mg/Al molar ratios [19]. This hydromagnesite is the main source of MgO via the following reaction:

$$Mg_5(CO_3)_4(OH)_2 \cdot 5H_2O \xrightarrow{500\ ^\circ C} 5MgO + 4CO_2 + 6H_2O$$

The lowering of the intensity and the broadening of the band of MgO reflections at lower Mg/Al molar ratio can also be due to the higher content of an amorphous mixed oxide phase possibly in the

form of Mg(Al)O and the fact that less microcrystalline MgO is present.

Fig. 2 shows the IR spectra of LDH and CLDH with a Mg/Al molar ratio of 5.6 (note: other ratios showed similar trends) [22]. The vibration at 1421 cm^{-1} is due to the asymmetric stretching mode (ν_3) of free CO_3^{2-}, while the vibration (ν_3) at 1384 cm^{-1} indicates the presence of CO_3^{2-} in the interlayer space. A further band at 1482 cm^{-1} signifies different vibration modes of CO_3^{2-}. These vibrations could also indicate the lowering of the symmetry of CO_3^{2-} from D_{3h} to C_{2v}. The vibration at 1635 cm^{-1} could indicate the presence of physically adsorbed water as the bending vibration of H_2O molecules appears in this region [23–25]. The presence of water even when the material was heated at a relatively high temperature (Fig. 2b) is not surprising as a previous study [26] reported the desiccant property of calcined LDH that could lead to adsorption of atmospheric H_2O molecules. One can observe that after calcination of LDH at 500 °C, the relative intensity of the vibration at 1384 cm^{-1} has increased, cf. other vibrations. This peak could be due to interlayer CO_3^{2-} from hydromagnesite and could indicate that not all hydromagnesites decomposed upon calcination. The intensity of this vibration was found to increase with Mg/Al ratio indicating that the amount of hydromagnesite is increasing. Vibrations at 1421 cm^{-1} and 1482 cm^{-1} on the other hand almost disappeared after calcination (Fig. 2b). This shows that free CO_3^{2-} is mostly removed and provides further evidence for the proposal that the 1384 cm^{-1} vibration for CLDH comes mostly from undecomposed hydromagnesite. Previous work in our laboratory has shown that these vibrations become more apparent as the Mg/Al molar ratio increases [22]. TGA analysis revealed that following calcination (500 °C) further heating of the material up to 800 °C caused a further weight loss of ca. 4% (see Supplementary information). This weight loss could be due to further decarbonation of the material. The TGA curves also indicated that more CO_3^{2-} ions are present and less surface bound water for LDH with Mg/Al = 5.6 when compared to the LDH with Mg/Al = 3.1.

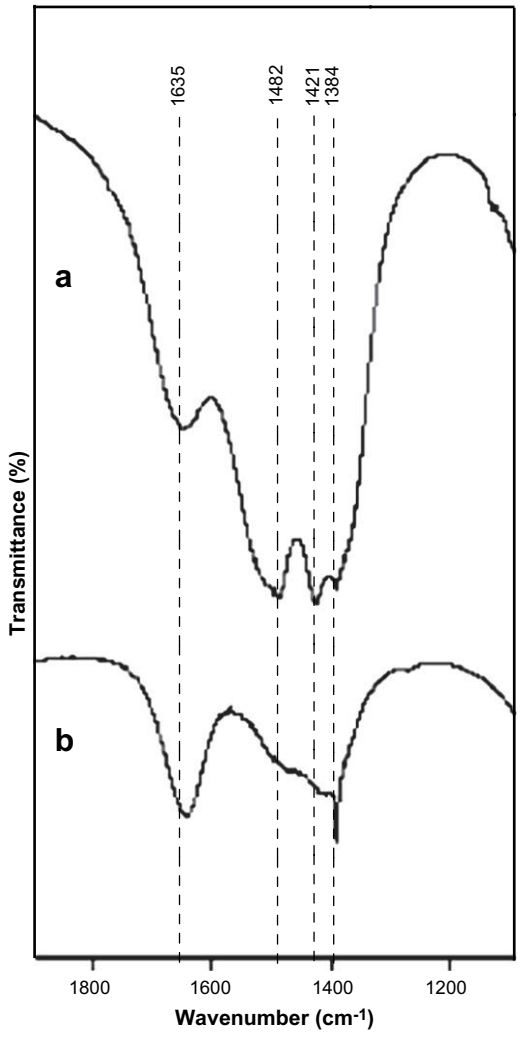

Fig. 2. FT-IR spectra of: (a) LDH and (b) CLDH at Mg/Al molar ratio of 5.6.

3.2. Adsorption experiments

Preliminary tests on CLDH materials indicated that these materials have an excellent affinity for AB9 at Mg/Al ≥3.0 (see Supplementary information). Most importantly, the dye affinity of the calcined products to AB9 was in all cases significantly higher than that for the uncalcined precursor. This result is consistent with previous studies that used different anionic adsorbates and LDHs of different compositions. For example: (1) Hussein et al. [6] reported that the adsorption capacity of the calcined (500 °C) product is higher than that of the uncalcined precursor for a Mg–Al-carbonate system with Mg/Al atomic ratio = 4 and "Mikethrene Olive Green B" dye; (2) Ulibarri et al. [7] demonstrated that a calcined (500 °C) hydrotalcite-like compound with a formula of $[Mg_3Al(OH)_8]_2CO_3 \cdot xH_2O$ is more effective in removing trichlorophenol and trinitrophenol from the solution compared with the uncalcined precursor; (3) Zhu et al. [27] showed that a calcined Mg–Al LDH with a Mg/Al molar ratio of 2:1 (500 °C) had a higher sorption capacity towards "Brilliant Blue R" than the uncalcined precursor; (4) Géraud et al. [28] also reported that the adsorption capacities of $[Mg_{2.0}Al(OH)_6]_{0.5}CO_3 \cdot nH_2O$ macroporous structures are very high, particularly for the calcined (450 °C) material compared with the uncalcined precursor whereby an Orange II azo dye was used as adsorbate; and (5) Das et al. [29] found that of various calcined LDHs, such as Mg–Al, Zn–Al, Ni–Al, Co–Al, Mg–Fe, Zn–Fe, Ni–Fe and Co–Fe (500 °C), the Mg–Al LDH with a Mg/Al molar ratio of 2.0 showed higher adsorption phosphate capacity compared with higher Mg/Al molar ratio (3.0 and 4.0) but no comparison was made with the uncalcined precursor.

In our previous study, optimum adsorption of AB9 was achieved by LDHs with Mg/Al molar ratios varying from 3.1 to 4.4 [19]. In the case of CLDHs, initial dye affinity tests indicated particularly strong adsorption for materials with Mg/Al ratios of 3.1–7.6. Further quantitative study of these materials was undertaken which involved measuring the adsorption isotherms. Figs. 3 and 4 show the adsorption isotherms for AB9 binding to the CLDH at different Mg/Al molar ratios using 20% (v/v) glycerol–H_2O and pure water solvent systems. The data was were fitted to the Langmuir model that allowed the maximum adsorption capacities (C_m) and binding constants (K_a) to be estimated. It should be pointed out that other models, such as Freundlich and Temkin, were tested but the fit to the data was not as satisfactory when compared to the Langmuir model. This analysis represents an approximation and in some cases there were deviations between the observed and the fitted curves. For some materials, the adsorptive capacity does not plateau but continues to slowly increase as the relative dye concentration is increased (see Fig. 3). This behavior was more obvious in the case of glycerol–water solvent than for pure water (see Fig. 4). In terms of the general shape of the isotherms, the curves are of L-2 type indicating that AB9 ions are adsorbed onto the surface by strong interactions that reach a "saturation value" represented by the "plateau" of the isotherm. Further to this, the initial part of the isotherm is nearly vertical indicating a strong chemisorption interaction. Thus, AB9 has a very high affinity for these materials for both solvent systems, and these isotherms can

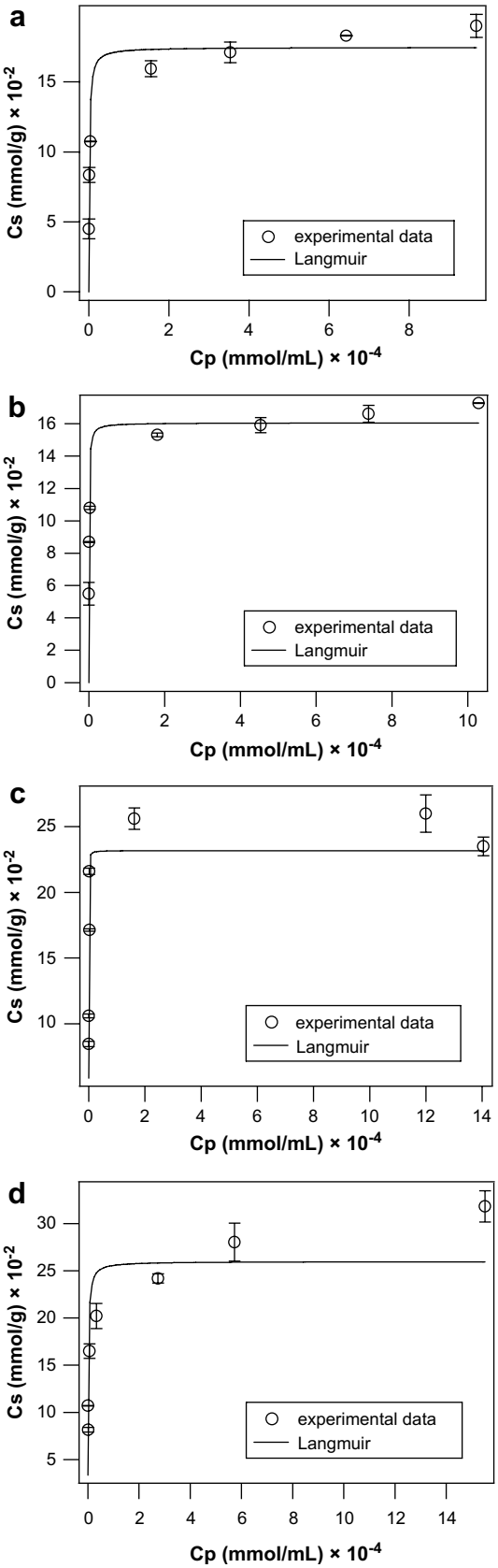

Fig. 3. Adsorption isotherm for 1.85 mM AB9 binding to CLDH with Mg/Al molar value equal to: (a) 3.1, (b) 4.4, (c) 5.6 and (d) 7.6. The solvent system is 20% (v/v) glycerol–H_2O and adsorption was conducted at ambient temperature.

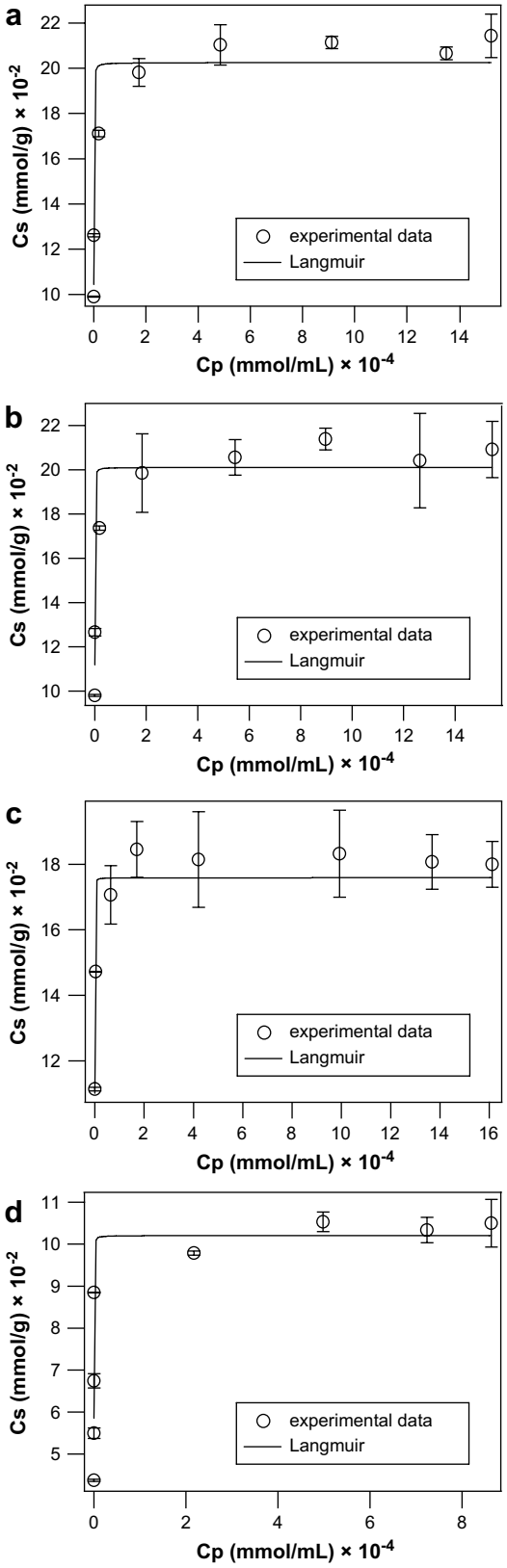

Fig. 4. Adsorption isotherm for 1.85 mM AB9 binding to CLDH with Mg/Al molar value equal to: (a) 3.1, (b) 4.4, (c) 5.6 and (d) 7.6. The solvent system is pure H_2O and adsorption was conducted at ambient temperature.

also be classified as an H-2 type, an extreme case of L-type isotherms. The deviation between the fitted data and experimental data at the higher dye concentration especially for 20% (v/v) glycerol–H_2O solvent may be indicating that multiple adsorption mechanisms are involved, as may be expected for such heterogeneous materials, or further adsorption processes (most likely intercalation) may take place at higher dye concentrations.

Given the heterogeneity of these materials, different types of adsorption sites and the possibility of surface adsorption and partial/full intercalation, it is not surprising to find that strict Langmuir behavior is not observed (note again that poorer fits were obtained with other commonly used models for adsorption behavior (*vide supra*)). Despite these complications, the parameters determined from the Langmuir fitting offer useful insights into the variation in adsorption behavior with composition. Recent studies using different adsorbent–adsorbate systems have shown similar trends of adsorption behavior [30–32]. These workers have pointed out that the Langmuir model gives a more satisfactory fitting of the data compared with other models. The calculated Langmuir model parameters (C_m and K_a) are given in Table 1. Two trends can be observed: (1) the maximum monolayer coverage (C_m) of all CLDHs studied increased significantly compared with the LDH precursors; and (2) there is a direct relationship between the molar ratio and C_m for the 20% (v/v) glycerol–H_2O solvent, i.e., as the Mg/Al molar ratio increases so do the C_m values; on the other hand the opposite is true for pure water. For the glycerol-containing solvent, materials with Mg/Al molar ratios of 3.1 and 4.4 gave the same C_m value of ca. 0.17 mmol/g. This value increased by a factor of 1.4 when the Mg/Al molar ratio is 5.6, giving a C_m of 0.23 mmol/g followed by a smaller increase for the Mg/Al of 7.6. An optimum value for the K_a was observed for CLDH with Mg/Al = 5.6 ($K_a \approx 1 \times 10^7\ M^{-1}$). For pure water, Mg/Al = 3.1 and 4.4 gave the highest C_m value of 0.20 mmol/g. This value decreased marginally when the Mg/Al was 5.6 ($C_m = 0.18$ mmol/g) and more significantly for the material with Mg/Al = 7.6 ($C_m = 0.10$ mmol/g). Interestingly, all K_a values have increased significantly (3- to 35-fold) for the pure water as solvent when compared to the glycerol-containing solvent for all the Mg/Al ratios. Although the C_m value is not at a maximum at Mg/Al = 5.6 in pure H_2O, this CLDH material exhibits the best adsorption properties in terms of dye affinity, as measured by K_a. Furthermore, using the same solvent, the C_m value for Mg/Al = 5.6 increased almost four-fold while the K_a value is about 140 times greater compared to the LDH precursor. Overall, the K_a values for the CLDHs are much higher than those measured for the uncalcined LDHs.

The contradictory trend between the C_m and Mg/Al values of CLDH using different solvent systems is worthy of comment. In pure water, the results are in agreement with the previously mentioned results of Das et al. [29] and that the higher affinity (capacity) is due to a higher Al^{3+} content of CLDH (lower Mg/Al). In that study, however, the binding constants for different divalent/trivalent metal ratios were not reported. For the short contact time used in this study, adsorption is expected to primarily involve surface adsorption and not intercalation. Thus, for the glycerol-containing solvent, the trend reversal can be partially explained in terms of changes in solvent viscosity and swelling of CLDH in this medium, and in the ability of glycerolate anions to interact with oxide surfaces, both of which subtly change the AB9 adsorption process. In terms of dye uptake, glycerol has a more beneficial effect when the MgO content is highest, but the affinity constant (K_a) is significantly reduced. The effect of glycerol addition aside, the AB9 dye does bind strongly to the various oxide phases and has a good affinity for the Mg rich oxide phase produced on calcination.

3.3. Textural properties

The crystallization of MgO after calcination appears to enhance the AB9 affinity of CLDH materials. Previous studies [26,33,34] have found that calcined (500 °C) product of Mg–Al-LDH (mainly MgO) has more strong basic sites than alumina (Al_2O_3) but less than pure magnesia (MgO). At low initial Mg/Al, there would be less MgO in the CLDH product but with more Mg(Al)O mixed oxide phase that can be formed after calcination at 500 °C; this therefore can lead to less basic sites that may be responsible to less adsorption of AB9 (acidic). Theoretically, as the Mg/Al molar ratio is increased, more MgO should be found in the calcined product as shown in the powder X-ray diffractograms (see Supplementary information). A carbonate interlayer anion precursor therefore seemed to be a good choice, since Zhang et al. [35] reported that the surface basicity of the calcined LDH depends on the interlayer anions that increases progressively following the order: $SO_4^{2-} < NO_3^- < CO_3^{2-}$.

Fig. 5 shows the N_2 adsorption and desorption isotherms for some CLDH materials measured in this study. All materials exhibited type IV isotherms according to the classification of Sing et al. [36], which is typical for mesoporous materials. Characteristic features of this type of isotherm are its hysteresis loop, which is associated with capillary condensation taking place in mesopores, the limiting uptake over a range of high p/p^o and the initial part of the isotherm which is attributed to monolayer–multilayer adsorption. Hysteresis loops may exhibit a wide variety of shapes [36]. In the case of the CLDH materials studied, all exhibited an H-3 type which is similar to their corresponding uncalcined precursors.

This H-3 type loop does not exhibit any limiting adsorption at high p/p^o that could give some insights into the materials' surface topography which is an aggregate of plate-like particles giving rise to slit-shaped pores. This conclusion is supported by scanning electron microscopy. The inherent mesoporosity of these materials makes them highly suitable to be used as adsorbent for anionic dye molecules having a molecular size dimension between 5 and 20 Å. This means that for microporous (pore size <20 Å) materials, the pores might be too small for some larger dye molecules. On the other hand, for macroporous (pore size >500 Å) materials, this could also mean less adsorption because of the lower surface area. Only mesoporous materials will have the surface morphology capable of positioning the dye molecules with sizes ranging from 5 to 20 Å in such a way that highest interaction is possible, i.e., when the energy potential within the pore would be at the minimum [22].

Table 1
Langmuir model parameters for Acid Blue 9 binding to the LDH and CLDH systems at different Mg/Al ratios.[a]

Mg:Al molar ratio	LDH [19]		CLDH			
	Solvent: 20% (v/v) glycerol–H_2O		Solvent: 20% (v/v) glycerol–H_2O		Solvent: pure H_2O	
	C_m (mmol/g)	K_a (M^{-1}) × 10^5	C_m (mmol/g)	K_a (M^{-1}) × 10^5	C_m (mmol/g)	K_a (M^{-1}) × 10^5
3.1	0.076 (±0.003)	1.18 (±0.20)	0.175 (±0.013)	7.6 (±3.9)	0.202 (±0.006)	74 (±16)
4.4	0.075 (±0.002)	1.19 (±0.11)	0.161 (±0.014)	17 (±11)	0.201 (±0.006)	120 (±27)
5.6	0.061 (±0.001)	1.24 (±0.13)	0.232 (±0.018)	110 (±60)	0.176 (±0.005)	286 (±90)
7.6	–	–	0.260 (±0.026)	6.2 (±4.4)	0.102 (±0.008)	217 (±84)

[a] Determined by atomic absorption spectroscopy.

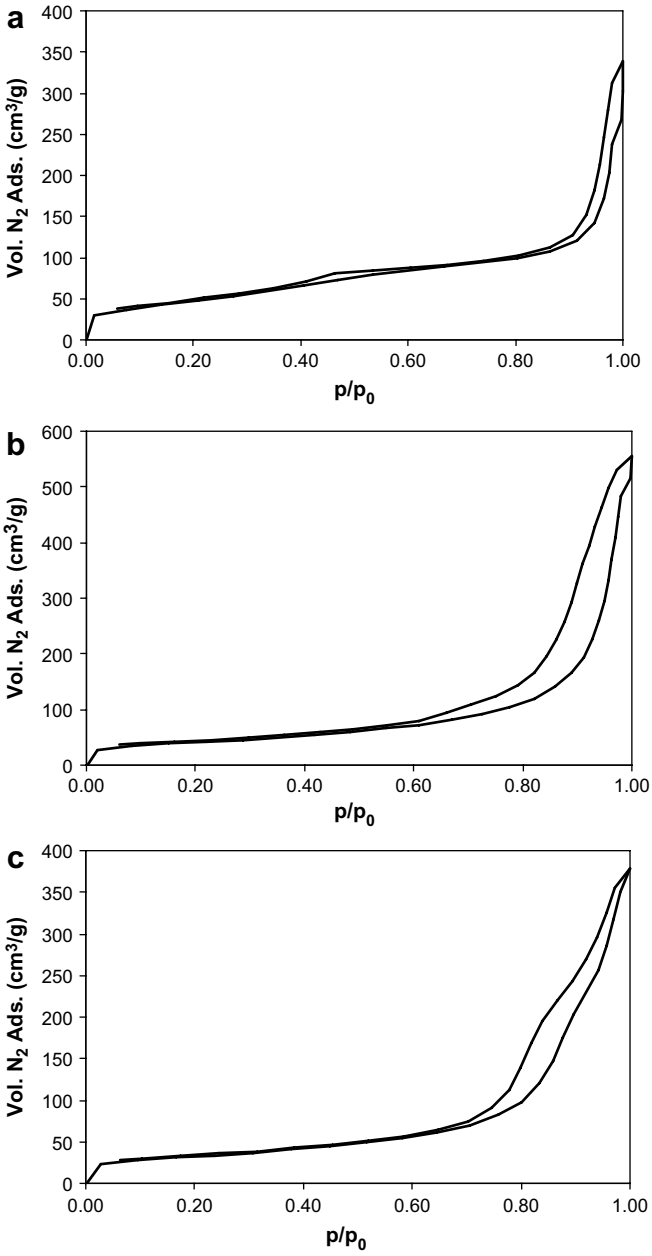

Fig. 5. N_2 adsorption–desorption isotherms of CLDH materials with Mg/Al molar ratio of: (a) 1.9, (b) 4.4 and (c) 10.7.

The adsorption behavior can be further rationalized by examining the textural property of these materials. Table 2 shows the experimental textural properties of LDH [19] and CLDH at varying Mg/Al molar ratio values. In general, the surface areas of all LDH precursors have increased dramatically after calcination at 500 °C. This could be the major factor responsible for the increase in AB9 affinity for all CLDHs compared with the original LDHs. However, it is quite remarkable that there is no direct correlation between AB9 affinity and the surface areas of CLDHs. For LDH precursors, it was emphasized [19] that those materials (Mg/Al = 3.0–5.6) having higher surface areas consequently exhibited high AB9 affinity. For the calcined products, however, all except the one with the lowest Mg/Al molar ratio (Mg/Al = 1.9) have higher AB9 affinity than the uncalcined LDHs. The adsorptive capacity does increase with Mg content (see Table 1). There was no correlation between the pore diameter and the adsorptive capacity of the CLDH materials. After calcination, each corresponding CLDH had a smaller pore size and higher surface area than their parent LDH. Like the LDHs, the CLDH materials exhibited mesoporosity (pores = 20–500 Å). The LDH with a Mg/Al molar ratio of 1.9 had the lowest pore size after calcination of all the materials produced and, for this material, could consequently result in its unusually low AB9 affinity in comparison to other CLDHs. Restricted access of AB9 anions to the inner part of the open pores and to the voids (space or interstice between particles) could reduce dye adsorption. Given that the CLDH with Mg/Al = 1.9 exhibited the lowest dye affinity in preliminary test and had the lowest pore volume value (0.42 cm^3/g), the pore volume can be a factor of dye adsorption properties aside from the surface area. All other CLDHs have pore volume values $\geq$0.5 cm^3/g and exhibited high dye affinity. However, no general trend can be found within these pore volume values of each CLDH in relation to the affinity of the material to AB9. Notably, the pore volumes of CLDHs for Mg/Al ratio >4.4 are substantially higher than that for the uncalcined LDH. This may be contributing to the higher dye affinity of the CLDHs. Finally, density measurements of all the materials showed an increase from ca. 2.0 g/cm^3 before calcination to ca. 3.2 g/cm^3 after calcination. Although there is no correlation between the CLDH densities and CLDH adsorptive behavior, this increase in density may be due to the presence of crystalline MgO in the calcined product. The lower density (3.2 g/cm^3) when compared with the pure MgO density (3.65 g/cm^3) [37] could be due to the presence of lower density amorphous material (possibly an aluminum phase which is crystalline at higher temperature) that formed on calcination at 500 °C of the LDH material.

Fig. 6 shows the scanning electron micrographs of all CLDH materials studied. Scanning electron microscopy has been applied

Table 2
Experimental textural properties of LDH and CLDH materials with variable Mg/Al ratios.

LDH [19]					CLDH			
Mg:Al molar ratio[a]	Surface area[b] (m^2/g)	Ave. pore diameter[c] (Å)	Corrected pore volume[c] (cm^3/g)	Average density[d] (g/cm^3)	Surface area[b] (m^2/g)	Average pore diameter[c] (Å)	Corrected pore volume[d] (cm^3/g)	Average density[d] (g/cm^3)
1.9	40	284	0.28	2.10	173	96	0.42	3.09
3.0	118	263	0.78	2.00	160	269	1.07	3.15
3.1	123	266	0.82	2.03	183	208	0.95	3.13
4.4	110	264	0.72	2.01	145	222	0.80	3.17
5.6	81	225	0.45	1.99	136	174	0.60	3.20
7.6	29	236	0.17	1.99	135	156	0.53	3.19
8.0	23	271	0.16	2.01	121	217	0.66	3.21
9.3	24	263	0.16	2.01	129	298	0.96	3.21
10.7	21	293	0.15	1.99	114	208	0.59	3.19

[a] Determined by AAS analysis.
[b] BET method.
[c] BJH method.
[d] Helium pycnometry.

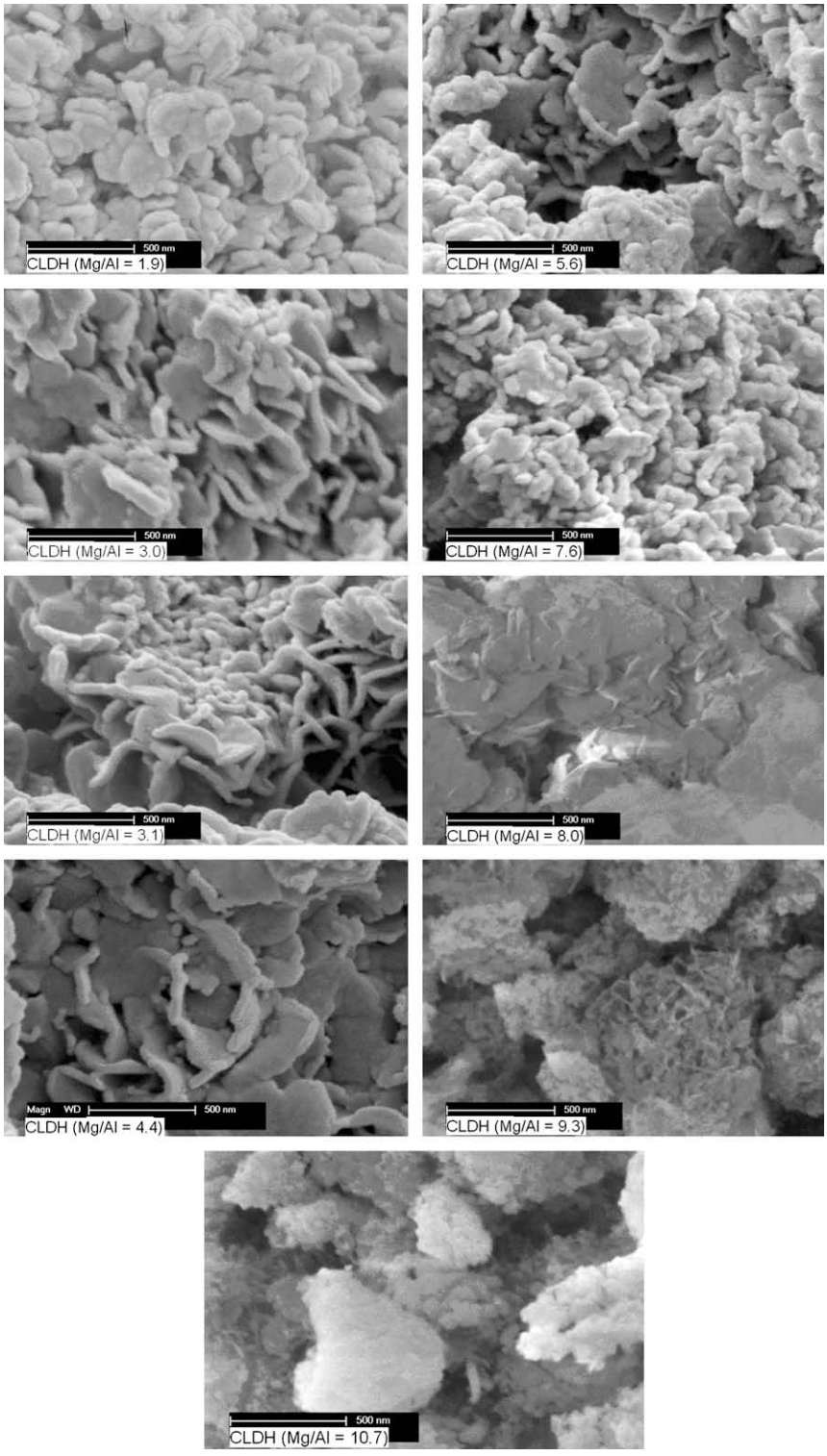

Fig. 6. Scanning electron micrographs of CLDH materials with different Mg/Al molar ratios.

to further elucidate changes in the shape, size and pore network of the LDHs on heating. SEM micrographs are consistent with the N_2 adsorption–desorption analysis. As mentioned before, the hysteresis loop exhibited by the CLDH materials suggests that it is an aggregate of plate-like particles with slit-shaped pores. In fact, the general hexagonal-shaped ($Mg/Al = 1.9$) and the platelet-like crystals ($Mg/Al \geq 3.0$) of the precursor LDHs were still observed in the calcined products (see Fig. 6). This is expected since both LDH precursor and CLDH calcined products gave the same N_2 adsorption–desorption analysis results. It was reported [38,39] that CO_2 and H_2O vapor evolution during thermal decomposition of a carbonate-containing LDH takes place through fine pores generated at the brucite-like layers leading to the formation of channels and chimneys, thus, accounting for the increase in specific surface area (higher AB9 affinity) observed for the medium-temperature calcined samples. In fact, holes created during CO_2 escape appeared

as small, regularly spaced craters (see Fig. 6 – ratio = 9.3 and 10.7). If pores are formed during CO_2 escape from the layers, then small pore formation is favorable when more carbonate is present in the interlayer, leading to higher surface area. In this study, this phenomenon occurs only when the Mg/Al molar value becomes very high (Mg/Al = 9.3 and 10.7) while all other materials generally retained their original surface morphology. This is in agreement with the result presented by Hibino et al. [40] who have shown that in samples with large Al content (minimum Mg/Al value), CO_2 evolution is observed even at 900 °C. They claimed that during collapse of the structure, some carbonates remain trapped inside the decomposed material, thus hindering complete decarbonation, which takes place only when Al^{3+} migrates to form $MgAl_2O_4$ spinel. For lower Al^{3+} content (maximum Mg/Al value), such a process would not be observed.

3.4. Adsorption mechanism

Earlier it was noted that the likelihood of dye intercalation through reconstruction may be possible, considering the continuing slow increase of dye adsorption as the relative dye concentration is increased (see Fig. 3). This is especially true when a swelling agent such as glycerol is included in the reacting mixture. To this end, we have varied the experimental conditions and have mainly utilized powder X-ray diffraction techniques to gain understanding about the possible adsorption mechanism. Firstly, the dye (in 20% (v/v) glycerol–H_2O) treated material during the dye affinity test was collected. This material was dried at 100 °C for 24 h, ground and subjected to PXRD analysis. Fig. 7 shows the diffractograms of CLDH materials after dye treatment and at the outset, the LDH precursor exhibited its "memory effect" by reconstructing to its original LDH structure as evident through the re-appearance of (003) and (006) reflections. These peaks were broadened and the intensity decreased compared with the original LDHs [19] indicating some reduction in crystallinity. Some crystalline MgO crystals remained (*double asterisks*) indicating that complete reconstruction did not occur, as may be expected given that Mg is in excess. However, the d_{003}-spacing increased from 7.8 Å (original LDH) to 9.8 Å (reconstructed LDH). An increase of only 2 Å cannot be attributed to intercalation of the AB9 dye taking into account the possible orientation of AB9 in the interlayer of the reconstructed LDH [19,20]. For our adsorption experiment conditions (low exposure time) only external surface adsorption appears to have occurred.

Secondly, the dye treatment conditions for our CLDH materials were varied. Figs. 8 and 9 show some X-ray powder diffractograms for CLDH with Mg/Al = 3.1 and 5.6 under different treatment conditions. Both figures show a slight increase in the basal spacing which is likely to be due to the presence of glycerol (see Figs. 8c and 9c). Glycerol intercalation produced an uneven expansion of the LDH layer with very low crystallinity. To probe whether longer exposure to the solvent and the dye will allow AB9 to intercalate, representative CLDH materials (Mg/Al = 3.1 and 5.6) were exposed to the same dye concentration and solvent system for 24 h with occasional stirring (Figs. 8a and 9a). Surprisingly, no substantial increase in the basal spacing could be observed. This strengthens our earlier claims that intercalation of AB9 has not occurred for even with longer exposure time, the basal spacing could not correspond to AB9 intercalates. The powder XRD for reconstructed LDH was very similar to the original LDH when the solvent is pure water (see Figs. 8b and d, 9b and d). But some reflections such as (003) and (006) shifted to lower angle for the glycerol-containing solvent (see Figs. 8c and 9c).

Finally, when 0.05 g of CLDH (Mg/Al = 5.6) was tested for its affinity to AB9 (5 mL; 1.85 mM) solutions with solvents, pure water and 20% (v/v) glycerol–water, the same relative absorbance was observed of such material for the two solvent systems giving a value of 0.49 (±0.08). Interestingly, when the mixture (after

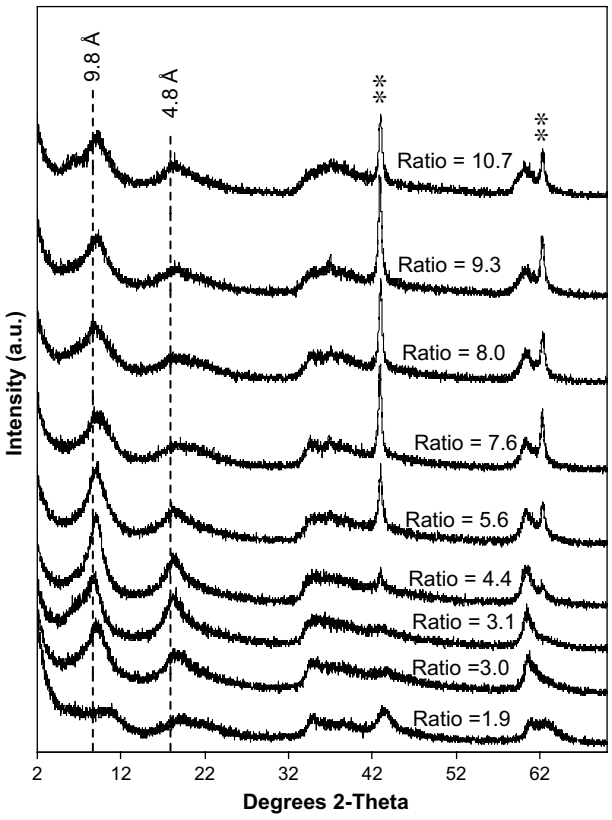

Fig. 7. X-ray powder diffractograms of CLDH systems after treatment of Acid Blue 9 (1.85 mM) in 20% (v/v) glycerol–water solvent system.

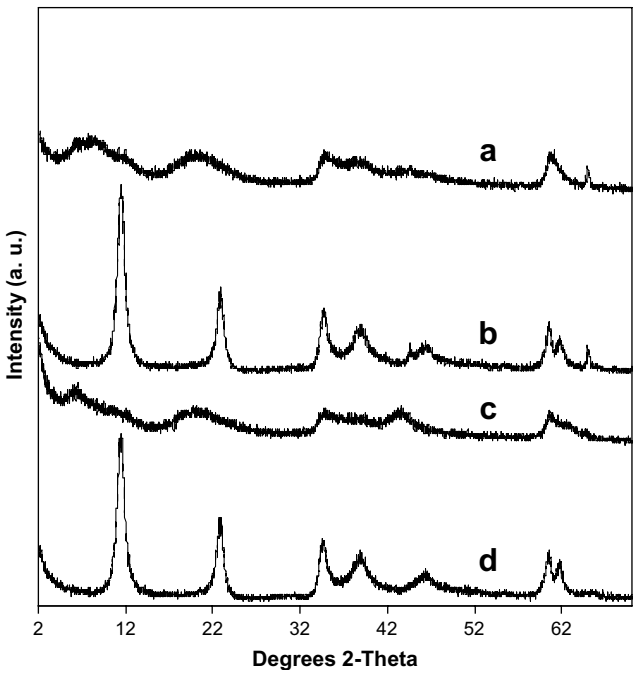

Fig. 8. X-ray powder diffractograms of CLDH with Mg/Al = 3.1 upon treatment of: (a) 1.85 mM AB9 in 20% (v/v) glycerol–H_2O and left for 24 h; (b) 1.85 mM AB9 in pure H_2O; (c) 20% (v/v) glycerol–H_2O and (d) pure H_2O.

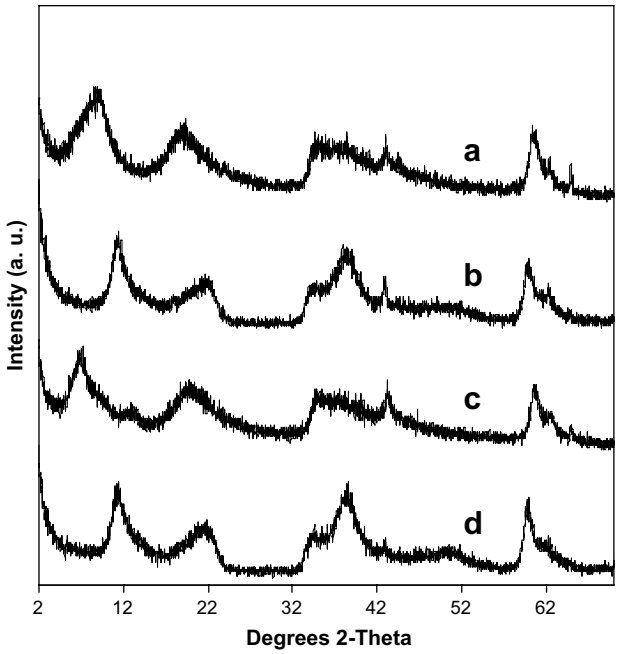

Fig. 9. X-ray powder diffractograms of CLDH with Mg/Al = 5.6 upon treatment of: (a) 1.85 mM AB9 in 20% (v/v) glycerol–H_2O and left for 24 h; (b) 1.85 mM AB9 in pure H_2O; (c) 20% (v/v) glycerol–H_2O and (d) pure H_2O.

centrifugation) was left for approximately one month, visible changes in the color of the supernatant liquid were observed, i.e., the intensity of the blue color becomes almost negligible (clear solution) especially for glycerol-containing solvent. The precipitate was then collected and dried at 100 °C for 24 h for PXRD analysis. Fig. 10 shows the X-ray powder diffractograms of the precipitate recovered (originally containing CLDH with Mg/Al = 5.6) for both solvent systems. Essentially, the original LDH structure was reconstructed when pure H_2O solvent was used giving virtually the same basal spacing of ca. 8.0 Å (see Fig. 10a) as the original LDH [19]. Reflections (9.6°, 13.8°, 15.2°, 19.9°, 21.2°, 30.8° and 41.9°) due to hydromagnesite in the original LDH have disappeared, instead MgO reflections at 44.4° and 64.7° (shown by arrow) emerged for

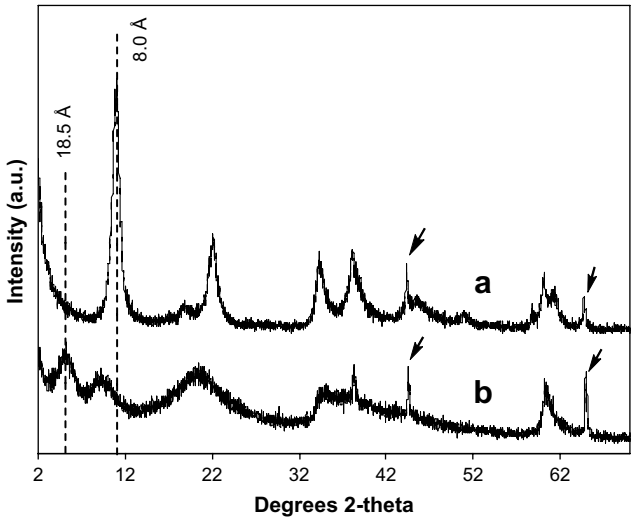

Fig. 10. X-ray powder diffractograms of CLDH with Mg/Al = 5.6 upon treatment with 1.85 mM AB9 in: (a) pure H_2O and (b) 20% (v/v) glycerol–H_2O. Note: conditions used were as for the dye affinity test but after centrifugation, the mixture was left for a month before the precipitate was recovered.

reasons previously discussed. This means that hydromagnesite materials, unlike hydrotalcite do not have the ability to reconstruct themselves. In the case of glycerol-containing solvent, the (003) reflection of the reconstructed LDH has moved to a lower angle of ca. 4.8° that gave a basal spacing of ca. 18.5 Å. This result is in close agreement with our previous study [19] and it can be concluded that, in this case, AB9 ions have been intercalated.

4. Conclusions

The present investigation shows that C.I. Acid Blue 9 affinity and its uptake are greater in CLDH compared with their corresponding uncalcined LDH precursors for pure water and 20% (v/v) glycerol–H_2O solvent systems. The presence of MgO microcrystallites in the calcined product seems to influence the adsorption behavior due to the basic character of this compound and more carbonates can escape through the layer during calcination that resulted in small pore formation. The presence of glycerol had an adverse effect on dye adsorption. With pure water, the lower the Mg/Al molar ratio, the greater is the AB9 adsorption; but with the presence of glycerol, the opposite is found. Although the trend of the binding affinity was not affected by the presence of glycerol, the K_a in pure water is more than twice as much as the K_a obtained in glycerol-containing solvent. CLDH adsorbents exhibited an adsorption isotherm that was satisfactorily fitted using the Langmuir equation giving an L-2 type curve. At conditions used in the adsorption experiments, powder XRD analysis indicated that only surface adsorption occurs for CLDH. Although reconstruction of the original LDH precursors was observed, no intercalation of C.I. Acid Blue 9 was observed when the CLDH material was exposed to water or 20% (v/v) glycerol–water for a relatively short period of time. However, dye intercalation can occur provided a swelling agent such as glycerol is used and given a sufficient exposure time (at least one month). Finally, optimum dye adsorption was achieved for CLDH using an LDH precursor with Mg/Al = 5.6. This Mg/Al molar ratio optimized material gave a $C_m = 0.23$ mmol/g and a $K_a = 1 \times 10^7\ M^{-1}$ with 20% (v/v) glycerol–H_2O solvent. This value is almost 100-fold higher than that measured for the uncalcined LDH. In pure water, the corresponding C_m value is 0.18 mmol/g and the K_a value is ca. $3 \times 10^7\ M^{-1}$. The high affinity for anionic dyes indicates that these could prove interesting materials for use as ink receptor layers in inkjet print media.

Acknowledgements

This research was supported by the Smartprint Cooperative Research Centre (CRC), Australia. ARA thanks Monash University for a Postgraduate Publication Award.

Appendix. Supplementary information

It includes X-ray powder diffractograms of CLDH materials (Fig. S1), TGA plots of LDH materials (Fig. S2) and preliminary dye adsorption tests (Fig. S3). Supplementary data associated with this article can be found in the online version, at doi: 10.1016/j.dyepig.2008.09.011.

References

[1] Yang RT. Adsorbents: fundamentals and applications. New Jersey: John Wiley & Sons Inc.; 2003. p. 1.
[2] Cantu M, Salinas EL, Valente JS, Montiel R. Environ Sci Technol 2005;39:9715.
[3] Wang SL, Hseu RJ, Chang RR, Chiang PN, Chen JH, Tzou YM. Colloids Surf A 2006;277:8.
[4] Tsai WT, Chang CY, Ing CH, Chang CF. J Colloid Interface Sci 2004:72.
[5] Ulibarri MA, Pavlovic I, Barriga C, Hermosin MC, Cornejo J. Appl Clay Sci 2001;18:17.
[6] Hussein MZ, Zainal Z, Yaziz I, Beng TC. J Environ Sci Health 2001;4:565.

[7] Ulibarri MA, Pavlovic I, Hermosin MC, Cornejo J. Appl Clay Sci 1995;10:131.
[8] Lv L, He J, Wei M, Duan X. Ind Eng Chem Res 2006;45:8623.
[9] Ni Z-M, Xia S-J, Wang L-G, Xing F-F, Pan G-X. J Colloid Interface Sci 2007;316:284.
[10] Tsotsis TT, Sahimi M, Fayyaz-Najafi B, Harale A, Park B-G, Liu PKT. United States; 2007.
[11] Ito K, Fujiwara Y. US Patent 6,281,270 B1; 2001.
[12] Kengo I, Yoshio F. US Patent 6,281,270; 2001.
[13] Klass CP, Joyce MK. US Patent 6,616,748; 2003.
[14] Majumdar D, Schwark DW, Kress RJ, Blanton TN. US Patent 6,680,108 B1; 2004.
[15] Ulibarri MA, Hermosin MdC. Layered double hydroxides in water decontamination. In: Rives V, editor. Layered double hydroxides: present and future. New York: Nova Science Publishers; 2001.
[16] Li F, Wang Y, Yang Q, Evans DG, Forano C, Duan X. J Hazard Mater 2005;B125:89.
[17] Rives V. Study of layered double hydroxides by thermal methods. In: Rives V, editor. Layered double hydroxides: present and future. New York: Nova Science Publishers; 2001.
[18] Ulibarri MA, Labajos FM, Rives V, Trujillano R, Kagunya W, Jones W. Inorg Chem 1994;33.
[19] Auxilio AR, Andrews PC, Junk PC, Spiccia L, Neumann D, Raverty W, et al. Polyhedron 2007;26:3479.
[20] Auxilio AR, Andrews PC, Junk PC, Spiccia L, Neumann D, Raverty W, et al. J Mater Chem 2008;18:2466.
[21] Langmuir I. J Am Chem Soc 1918;40:1361.
[22] Auxilio AR. Ph.D. thesis, Monash University; 2007.
[23] Cavani F, Trifiro F, Vaccari A. Catal Today 1991;11:173.
[24] Costa FR, Leuteritz A, Wagenknecht U, Jehnichen D, Hauber L, Heinrich G. Appl Clay Sci 2008;38:153.
[25] Kloprogge JT, Frost RL. Infrared and Raman spectroscopic studies of layered double hydroxides (LDHs). In: Rives V, editor. Layered double hydroxides: present and future. New York: Nova Science Publishers, Inc.; 2001.
[26] Occelli ML, Olivier JP, Auroux A, Kalwei M, Eckert H. Chem Mater 2003;15:4231.
[27] Zhu M-X, Li Y-P, Xie M, Xin H-Z. J Hazard Mater 2005;B120:163.
[28] Géraud E, Bouhent M, Derriche Z, Leroux F, Prevot V, Forano C. J Phys Chem Solids 2007;68:818.
[29] Das J, Patra BS, Baliarsingh N, Parida KM. Appl Clay Sci 2006;32:252.
[30] Akkaya G, Ozer A. Process Biochem 2005;40:3559.
[31] Carriazo D, Arco Md, Martin C, Rives V. Appl Clay Sci 2007;37:231.
[32] Hu Q, Xu Z, Qiao S, Haghseresht F, Wilson M, Lu GQ. J Colloid Interface Sci 2007;308:191.
[33] Auroux A. Top Catal 1997;4:71.
[34] Gervasini A, Fenyvesi J, Auroux A. Langmuir 1996;12:5356.
[35] Zhang L, Zhu J, Jiang X, Evans DG, Li F. J Phys Chem Solids 2006;67:1678.
[36] Sing KSW, Everett DH, Haul RAW, Moscou L, Pierotti RA, Rouquerol J, et al. Pure Appl Chem 1985;57:603.
[37] Feng B, An H, Tan E. Energy Fuel 2007;21:426.
[38] Reichle WT, Kang SY, Everhardt DS. J Catal 1986;101:352.
[39] Tichit D, Medina F, Coq B, Dutarte R. Appl Catal A 1997;159:241.
[40] Hibino T, Yamashita Y, Kosuge K, Tsunashima A. Clays Clay Miner 1995;43:427.